

15 Entanglement in Many-Body Systems

Frank Pollmann
Technical University of Munich
Garching

Contents

1	Introduction	2
2	Many-body entanglement	2
2.1	Area law	4
2.2	Entanglement in free-particle models	6
3	Efficient representation and matrix-product states (MPSs)	7
3.1	Simple examples of MPS	9
3.2	Area law and MPS	10
3.3	Canonical form	11
3.4	Time Evolving Block Decimation (TEBD)	12
4	Symmetry-protected topological (SPT) phases	15
4.1	Projective representations	15
4.2	MPS representations of SPT phases	17
4.3	Simple examples of different SPT phases	17
4.4	Degeneracies in the entanglement spectrum	18
5	Universal entanglement scaling at critical points	19
6	Case study: Phase diagram of a spin-1 chain	20
7	Conclusions and further developments	22

1 Introduction

The notion of quantum entanglement goes back to the early years of quantum mechanics and was subject of several papers by Schrödinger [1]. At the same time Einstein, Podolsky, and Rosen discussed their famous “Gedankenexperiment” that attempted to show that quantum mechanical theory was incomplete [2]. Quantum entanglement is a physical phenomenon that occurs when particles interact in a way such that the quantum state of each particle cannot be described independently of the state of the others—including when the particles are separated by a large distance. For a long time, it was a topic discussed mostly in quantum optics and for systems with few degrees of freedom. In the last decades, however, it has seen a revival with input from very different areas, including the theory of black holes, quantum information and communication, the numerical investigation of quantum-many body systems, as well as the characterization of topological quantum states and quantum phase transitions.

In this chapter, we will introduce some basics of many-body entanglement and focus on a few selected applications. We begin by introducing basic notions of entanglement in many-body systems and discuss the *area law*, which is commonly obeyed by ground states of local Hamiltonians [3]. We then discuss different concepts in which the area law and the resulting locality of the ground state turn out to be extremely helpful for the investigation of quantum-many body phenomena: First, we show that one-dimensional area law states can be represented using matrix-product states (MPSs), allowing for efficient simulations of ground state properties and time-evolution [4, 5]. Second, we investigate the entanglement properties of gapped ground states and how they transform under symmetries, providing a framework for the classification of SPT phases [6, 7]. Third, we identify universal scaling properties of the entanglement entropies that allow us to characterize quantum phase transitions [8]. Finally we show how to apply all the concepts above to investigate the phase diagram of a spin-1 chain.

2 Many-body entanglement

In the following, we introduce the concept of entanglement entropy and entanglement spectra in many-body systems. Let us consider the bipartition of the Hilbert space $\mathcal{H} = \mathcal{H}_A \otimes \mathcal{H}_B$ of an N -body quantum system as illustrated in Fig. 1(a), where \mathcal{H}_A (\mathcal{H}_B) describes all the states defined in subsystem A and B , respectively.

We perform a so-called *Schmidt decomposition*, in which we decompose a (pure) state $|\Psi\rangle \in \mathcal{H}$ as

$$|\Psi\rangle = \sum_{\alpha} \Lambda_{\alpha} |\alpha\rangle_A \otimes |\alpha\rangle_B, \quad |\alpha\rangle_{A(B)} \in \mathcal{H}_{A(B)}, \quad (1)$$

where the states $\{|\alpha\rangle_{A(B)}\}$ form an orthonormal basis of (the relevant subspace of) \mathcal{H}_A (\mathcal{H}_B) and $\Lambda_{\alpha} \geq 0$. The Schmidt decomposition is unique up to degeneracies and for a normalized state $|\Psi\rangle$ we find that $\sum_{\alpha} \Lambda_{\alpha}^2 = 1$. Note that the Schmidt decomposition is equivalent to the singular-value decomposition of the coefficient matrix ψ_{ij} for chosen local bases $|i\rangle_A$ and $|i\rangle_B$, respectively. An important aspect of the Schmidt decomposition is that it gives direct insight

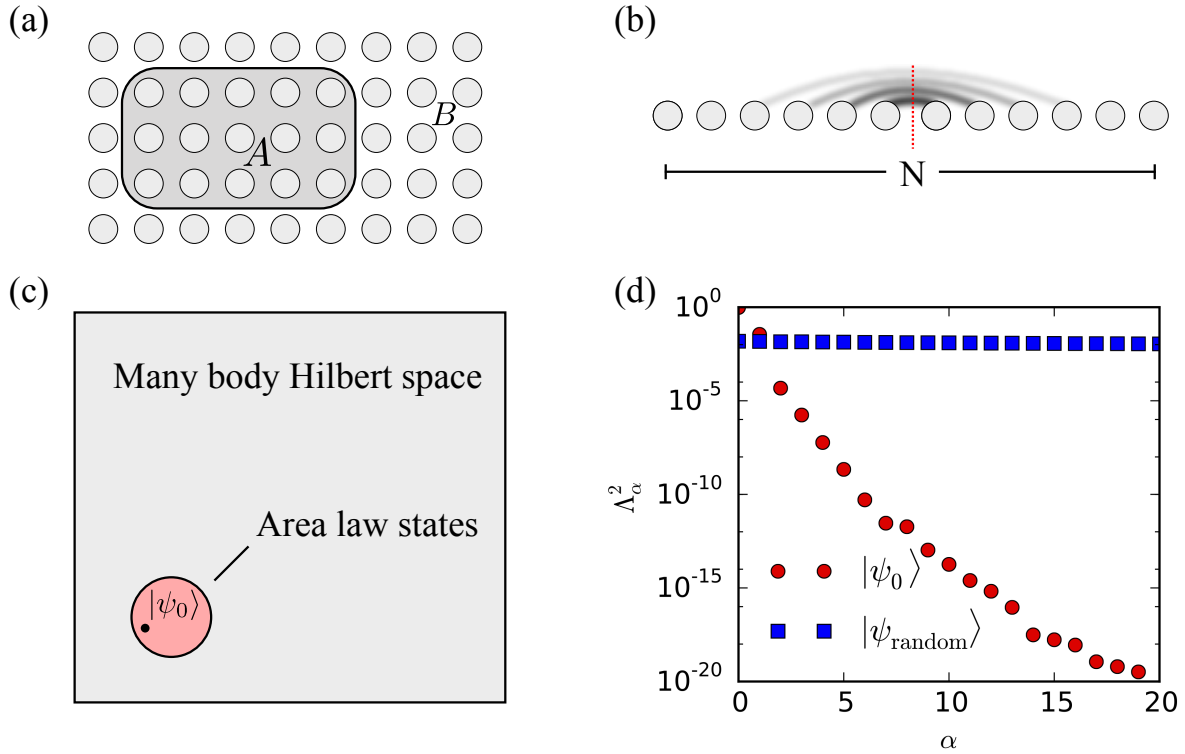


Fig. 1: (a) Bipartition of a system into two parts A and B . The shaded area A has a boundary ∂A of with surface area $|\partial A|$. (b) Significant quantum fluctuations in gapped ground states occur only on short length scales. (c) 1D area law states make up a very small fraction of the many-body Hilbert space but contain all gapped ground states. (d) Comparison of the largest Schmidt values of the ground state of the transverse field Ising model ($g = 1.5$) and a random state for a system consisting of $N = 16$ spins. The index α labels different Schmidt values.

into the *bipartite entanglement* (i.e., the quantum entanglement between degrees of freedom in \mathcal{H}_A and \mathcal{H}_B) of a state: If no entanglement between the two subsystems is present, the state is a *product state* and the Schmidt decomposition has only one single non-zero Schmidt value ($\Lambda_1 = 1$ and $\Lambda_{\alpha>1} = 0$). If the degrees of freedom of the two subsystems are entangled, we necessarily have multiple non-zero Schmidt values in the decomposition.

A useful measure to quantify the amount of entanglement is the so-called *entanglement entropy*, which is defined as the von-Neumann entropy $S = -\text{Tr}(\rho_A \log(\rho_A))$ of the reduced density matrix ρ_A . The *reduced density matrix* of an entangled (pure) quantum state $|\psi\rangle$ is the density matrix of a mixed state defined on the subsystem,

$$\rho_A \equiv \text{Tr}_B(|\psi\rangle\langle\psi|). \quad (2)$$

A simple calculation shows that it has the Schmidt states $|\alpha\rangle_A$ as eigenstates and the Schmidt coefficients are the square roots of the corresponding eigenvalues, i.e., $\rho_A = \sum_\alpha \Lambda_\alpha^2 |\alpha\rangle_A \langle\alpha|_A$ (equivalently for ρ_B). Hence, the entanglement entropy can be directly expressed in terms of the Schmidt values Λ_α ,

$$S = -\text{Tr}(\rho_A \log(\rho_A)) = -\sum_\alpha \Lambda_\alpha^2 \log \Lambda_\alpha^2. \quad (3)$$

Note that we would get the same entanglement entropy from the reduced density matrix ρ_B . If there is no entanglement between the two subsystems, we find $S = 0$; and $S > 0$ if there is any entanglement.

More generally, we can also consider Rényi entropies of the reduced density matrix

$$S_n = \frac{1}{1-n} \log \text{Tr} ((\rho_A)^n). \quad (4)$$

For the special case $n \rightarrow 1$, we recover the von-Neumann entropy. In analogy to the entanglement entropy, we find $S_n > 0$ for an entangled and $S_n = 0$ for an unentangled state for all n . Rényi entropies with integer n have the advantage that they can be evaluated by introducing n replicas—a tool that was originally introduced in analytical calculations [9]. This technique is also suitable to obtain Rényi entropies for Monte Carlo simulations [10] or even experimentally [11, 12]

Another useful quantity is the so-called *entanglement spectrum* $\{\varepsilon_\alpha\}$ [13], which is defined in terms of the spectrum $\{\Lambda_\alpha^2\}$ of the reduced density matrix by $\varepsilon_\alpha = -2 \log \Lambda_\alpha$.

To demonstrate the concepts above, we consider a simple system consisting of two spin-1/2 with a bipartition in which the first spin is in subsystem A and the second in subsystem B .

The first example is a wave function

$$|\psi\rangle = \frac{1}{2} (|\uparrow\uparrow\rangle + |\uparrow\downarrow\rangle + |\downarrow\uparrow\rangle + |\downarrow\downarrow\rangle) \quad (5)$$

with Schmidt decomposition

$$|\psi\rangle = 1 \cdot \frac{1}{\sqrt{2}} (|\uparrow\rangle + |\downarrow\rangle) \otimes \frac{1}{\sqrt{2}} (|\uparrow\rangle + |\downarrow\rangle), \quad (6)$$

representing a product state with entanglement entropy $S = 0$. The second example is a wave function

$$|\psi\rangle = \frac{1}{2} (|\uparrow\downarrow\rangle + |\downarrow\uparrow\rangle) \quad (7)$$

with Schmidt decomposition

$$|\psi\rangle = \frac{1}{\sqrt{2}} \cdot (|\uparrow\rangle \otimes |\downarrow\rangle) + \frac{1}{\sqrt{2}} \cdot (|\downarrow\rangle \otimes |\uparrow\rangle), \quad (8)$$

representing a maximally entangled state with entanglement entropy $S = \log 2$.

2.1 Area law

As we will discuss now, ground states of (gapped) local Hamiltonians are very special with respect to their entanglement properties—they fulfill an *area* law. It turns out that this allows on one hand for efficient numerical simulations and on the other hand provides the basis for the characterization of universal properties of quantum phases.

Let us first mention that a “typical” state in the Hilbert space has a *volume law*, i.e., the entanglement entropy grows proportionally with the volume of the partitions. In particular, it has

been shown in Ref. [14] that in a system of N sites with on-site Hilbert space dimension d , a randomly drawn state $|\psi_{\text{random}}\rangle$ has an entanglement entropy of $S \approx N/2 \log d - 1/2$ for a bipartition into two parts of $N/2$ sites. Highly excited eigenstates of generic (ergodic) Hamiltonians typically show the same behavior.

In contrast, ground states $|\psi_0\rangle$ of gapped and local Hamiltonians follow an *area law*, i.e., the entanglement entropy grows proportionally to the area of the cut [3]¹

$$S = \alpha |\partial A| + \dots, \quad (9)$$

where α in the leading term is a non-universal coefficient and $|\partial A|$ denotes the surface area of the cut.

For the special case of a one dimensional chain of length N that is cut into two equal halves as shown in Fig. 1(b) this implies that $S(N)$ is constant for $N \gtrsim \xi$ (with ξ being the correlation length). This can be intuitively understood from the fact that a gapped ground state contains only fluctuations within the correlation length ξ and thus only degrees of freedom near the cut are entangled. A rigorous proof of the area law for 1D gapped and local Hamiltonians is given in Ref. [15]. Since typical states have a volume law, ground states are very special states and can be found within a very small corner of the Hilbert space, as illustrated in Fig. 1(c).

An important observation is that in slightly entangled states, only a relatively small number of Schmidt states contribute significantly to the weight of the state. This is demonstrated in Fig. 1(d) by comparing the largest 20 Schmidt values of an area law state and a volume law state for a bipartition of an $N=16$ chain into two half-chains. As an example of an area law state, we considered here the ground state of the transverse field Ising model

$$H = - \sum_n \sigma_n^z \sigma_{n+1}^z + g \sigma_n^x, \quad (10)$$

with σ_n^x and σ_n^z being the Pauli operators and $g > 0$. This \mathbb{Z}_2 symmetric model has a quantum phase transition at $g_c = 1$. As shown in Fig. 1(d) for a representative example of $g = 1.5$, the entire weight of the ground state is essentially contained in a few Schmidt states. Generic states fulfilling the area law show a similar behavior and thus the above observation provides an extremely useful approach to compress quantum states by truncating the Schmidt decomposition. In particular, for all $\varepsilon > 0$ we can truncate the Schmidt decomposition at some *finite* χ (independent of the system size) such that

$$\left\| |\psi\rangle - \underbrace{\sum_{\alpha=1}^{\chi} A_{\alpha} |\alpha\rangle_L \otimes |\alpha\rangle_R}_{|\psi^{\text{trunc}}\rangle} \right\| < \varepsilon \quad (11)$$

This particular property of area law states is intimately related to the matrix-product state (MPS) representation of 1D quantum states, as we will discuss in the next chapter. The situation is very different for a highly entangled (volume law) random state: All the Schmidt values are roughly constant for all $2^{N/2}$ states and thus the 20 dominant states contain a vanishing weight (assuming an equal weight of configurations, we find $A_{\alpha}^2 \approx 1/2^{N/2}$ per Schmidt state).

¹The condition of a gap can in certain cases be released but generically leads to sub-leading log corrections. In systems with a Fermi surface, the area law breaks down.

2.2 Entanglement in free-particle models

While it is generically very hard to obtain the entanglement entropy in many-body systems, it can be easily obtained for free-particle models [16, 17]. This is particularly useful as it allows us to study many interesting aspects of entanglement in various settings—for example, universal properties that might occur independently of the presence or absence of interactions.

For free-particle states, the reduced density matrix ρ_A of a bipartite system can be written as

$$\rho_A = \frac{1}{Z} e^{-\mathcal{H}_A}, \text{ with } \mathcal{H}_A = \sum_{i \in A} \varepsilon_i f_i^\dagger f_i, \quad (12)$$

where f_i^\dagger (f_i) creates (annihilates) a single particle with energy ε_i with respect to the so-called “entanglement Hamiltonian” \mathcal{H}_A . The constant Z ensures the correct normalization $\text{Tr } \rho_A = 1$. Note that \mathcal{H}_A is not simply the physical Hamiltonian H restricted to the subsystem A and therefore Eq. (12) is not a true Boltzmann formula.

Let us now consider a non-interacting fermionic Hamiltonian of the form

$$H = \sum_{i,j} t_{i,j} c_i^\dagger c_j. \quad (13)$$

For a given filling factor, the ground state is a Slater determinant describing the filled Fermi sea. Following Wick’s theorem, all many-particle correlation functions factorize into products of one-particle functions, for example

$$\langle c_i^\dagger c_j^\dagger c_k c_l \rangle = \langle c_i^\dagger c_l \rangle \langle c_j^\dagger c_k \rangle - \langle c_i^\dagger c_k \rangle \langle c_j^\dagger c_l \rangle. \quad (14)$$

We can thus write the reduced density matrix in the form

$$\rho_A = K \exp \left(- \sum_{i,j \in A} h_{i,j} c_i^\dagger c_j \right) \quad (15)$$

with some constant K . We now need to find a matrix $h_{i,j}$ chosen such that ρ_A reproduces the correct single-particle correlation function $C_{i,j} = \langle c_i^\dagger c_j \rangle$ for $i, j \in A$. This is done in a common diagonal representation of both matrices: We diagonalize $C_{i,j}$ in subsystem A with eigenvalues ζ_n and corresponding eigenstates $\varphi_n(i)$. The transformation

$$c_i = \sum_n \varphi_n(i) f_n \quad (16)$$

yields for the single-particle correlation function $\langle f_n^\dagger f_{n'} \rangle = \zeta_n \delta_{n,n'}$. To obtain this from the reduced density matrix ρ_A , the entanglement Hamiltonian \mathcal{H}_A must have the diagonal form Eq. (12) with the single-particle entanglement spectrum

$$\varepsilon_n = \log \left(\frac{1 - \zeta_n}{\zeta_n} \right). \quad (17)$$

The many body entanglement entropy is then given by the sum of the contributions of each fermionic mode

$$S = - \sum_n \left(\zeta_n \log \zeta_n + (1 - \zeta_n) \log(1 - \zeta_n) \right). \quad (18)$$

To demonstrate the ideas, we consider a model of spinless fermions on a 1D chain of N sites with periodic boundary conditions described by the Hamiltonian

$$H = -t \sum_j \left(c_j^\dagger c_{j+1} + H.c. \right). \quad (19)$$

The following simple Python script calculates the entanglement entropy for the ground state at half filling for a bipartition into two halves (i.e., $A \equiv 1 \dots N/2$ and $B \equiv N/2+1 \dots N$):

```
import numpy as np
N = 20
t = 1
H = np.zeros((N,N))
for i in range(N):
    H[i,np.mod(i+1,N)] = -t
    H[np.mod(i+1,N),i] = -t

E,U = np.linalg.eigh(H)
C = np.dot(U[:N//2,:N//2],np.conj(U[:N//2,:N//2].T))
z = np.linalg.eigvalsh(C)

print ("S = ",-np.sum(z*np.log(z) + (1-z)*np.log(1-z)))
```

3 Efficient representation and matrix-product states (MPSs)

We will now introduce MPSs, which allow for an efficient representation of area law states in 1D. When working with MPSs, it is very helpful to use a diagrammatic tensor representation, which is illustrated in Fig. 2 (a) and (b). In this notation, a tensor with n indices is represented by a symbol with n legs.

We consider a chain with N sites and label the local basis on site n by $|j_n\rangle$ with $j_n = 1, \dots, d$, e.g., for a spin-1/2 we have $d = 2$ local states $|\uparrow\rangle, |\downarrow\rangle$. Using the tensor product of local basis states, a generic (pure) quantum state can then be expanded as

$$|\psi\rangle = \sum_{j_1, j_2, \dots, j_N} \psi_{j_1 j_2 \dots j_N} |j_1, j_2, \dots, j_N\rangle. \quad (20)$$

Note that the order- N tensor ψ_{j_1, \dots, j_N} has d^N complex entries which makes it prohibitively expensive to store or manipulate exactly even for moderate system sizes. For example, even on a large supercomputer, a simple $S=1/2$ system with $d=2$ can only be simulated exactly for up to $N \approx 40$ sites. Since numerical investigations of quantum-many body systems often require much larger systems, it is important to find ways to “compress” the quantum states to a manageable size—this is exactly what we will be able to do using MPS!

3.1 Simple examples of MPS

To become more familiar with the MPS notation, let us consider a few examples.

Product state: The state $|\psi\rangle = |\varphi^{[1]}\rangle \otimes |\varphi^{[2]}\rangle \otimes \cdots \otimes |\varphi^{[n]}\rangle$ can easily be written in the form of Eq. (22); since it has no entanglement, the bond dimension is simply $\chi_n = 1$ on each bond and the 1×1 “matrices” are given by

$$M^{[n]j_n} = \left(\varphi_{j_n}^{[n]} \right). \quad (23)$$

Concretely, the ground state of the transverse field Ising model given in Eq. (10) at infinite field $g \rightarrow \infty$ is a product state $|\leftarrow \cdots \leftarrow\rangle \equiv \left(\frac{1}{\sqrt{2}} |\uparrow\rangle - \frac{1}{\sqrt{2}} |\downarrow\rangle \right) \otimes \cdots \otimes \left(\frac{1}{\sqrt{2}} |\uparrow\rangle - \frac{1}{\sqrt{2}} |\downarrow\rangle \right)$, which we write as an MPS using the same set of matrices on each site n ,

$$M^{[n]\uparrow} = \left(\frac{1}{\sqrt{2}} \right) \quad \text{and} \quad M^{[n]\downarrow} = \left(\frac{-1}{\sqrt{2}} \right). \quad (24)$$

For the Néel state $|\uparrow\downarrow\uparrow\downarrow \dots\rangle$, we need different sets of matrices on odd and even sites,

$$M^{[2n-1]\uparrow} = M^{[2n]\downarrow} = \left(1 \right) \quad \text{and} \quad M^{[2n-1]\downarrow} = M^{[2n]\uparrow} = \left(0 \right) \quad (25)$$

for $n = 1, \dots, N/2$.

Dimerized state: A product of singlets $\frac{1}{\sqrt{2}} \left(|\uparrow\downarrow\rangle - |\downarrow\uparrow\rangle \right) \otimes \cdots \otimes \frac{1}{\sqrt{2}} \left(|\uparrow\downarrow\rangle - |\downarrow\uparrow\rangle \right)$ on neighboring sites can be written with 1×2 matrices on odd sites and 2×1 matrices on even sites given by

$$M^{[2n-1]\uparrow} = \left(\frac{1}{\sqrt{2}} \quad 0 \right), \quad M^{[2n-1]\downarrow} = \left(0 \quad \frac{-1}{\sqrt{2}} \right), \quad M^{[2n]\uparrow} = \begin{pmatrix} 0 \\ 1 \end{pmatrix}, \quad M^{[2n]\downarrow} = \begin{pmatrix} 1 \\ 0 \end{pmatrix}. \quad (26)$$

Spin-1 AKLT state: Affleck, Kennedy, Lieb, and Tasaki (AKLT) [21] constructed a Hamiltonian for which the ground state is an exact MPS of bond dimension $\chi=2$. The Hamiltonian reads

$$H = \sum_j \vec{S}_j \vec{S}_{j+1} + \frac{1}{3} (\vec{S}_j \vec{S}_{j+1})^2 = 2 \sum_j \left(P_{j,j+1}^{S=2} - \frac{1}{3} \right), \quad (27)$$

where \vec{S} are spin $S = 1$ operators and $P_{j,j+1}^{S=2}$ is a projector onto the $S = 2$ sector of the spins on sites j and $j+1$. This model is in a topologically nontrivial phase with remarkable properties of the ground state—we will get into this later. To construct the ground state, we note that the projector $P_{j,j+1}^{S=2}$ does not give a contribution if we decompose the $S = 1$ spins on each site into two $S = \frac{1}{2}$ spins and form singlets between spins on neighboring sites, as illustrated in Fig. 2(d). While the ground state is unique on a ring with periodic boundary conditions, in a chain with open boundary conditions the $S = \frac{1}{2}$ spins on the edges do not contribute to the energy and thus lead to a 4-fold degeneracy of the ground state. Given the structure of the ground state, we can construct the corresponding MPS: We start by writing the product of singlets with the matrices of Eq. (26) and add arbitrary spin- $\frac{1}{2}$ states φ^L and φ^R on the left and right. We apply the projectors $P^{S=1}$ to map the two spin- $\frac{1}{2}$ onto the physical spin-1 site, and contract the three tensors on each site to obtain the MPS structure. For sites $1 < n < N$ in the bulk, we obtain

$$M^{[n]+1} = \sqrt{\frac{4}{3}} \begin{pmatrix} 0 & 0 \\ \frac{1}{\sqrt{2}} & 0 \end{pmatrix} \quad M^{[n]0} = \sqrt{\frac{4}{3}} \begin{pmatrix} \frac{1}{2} & 0 \\ 0 & -\frac{1}{2} \end{pmatrix} \quad M^{[n]-1} = \sqrt{\frac{4}{3}} \begin{pmatrix} 0 & -\frac{1}{\sqrt{2}} \\ 0 & 0 \end{pmatrix}. \quad (28)$$

Here, we included the factor $\sqrt{\frac{4}{3}}$ to normalize the MPS.

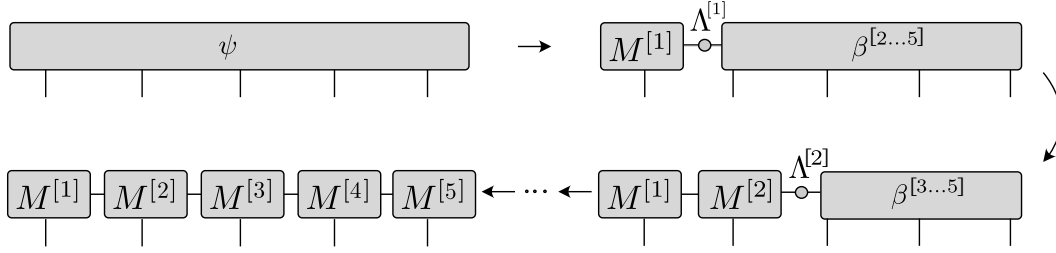


Fig. 3: Iterative conversion of a state $|\psi\rangle$ given by a rank- N tensor ψ_{i_1, \dots, i_N} using successive Schmidt decompositions in a diagrammatic representation. The horizontal lines represent the bond (Schmidt indices) $\alpha, \beta, \gamma, \dots$ and the vertical lines represent the physical indices $j_n \in \{1, \dots, d\}$. Connected lines between tensors denote summation over the corresponding indices (see text for details).

3.2 Area law and MPS

In general any state in a finite system can be decomposed *exactly* into the MPS form of Eq. (22). However, the caveat is that for a generic state (with a volume law entanglement), the required bond dimension $\chi_{\max} := \max_n \chi_n$ increases exponentially with the number of sites N . It turns out that all area law states can be very well approximated by MPS with a finite bond dimension χ_{\max} [22, 23].

For illustration, we will show now how a state can be brought into an MPS form starting from a full many-body state $|\psi\rangle$. For this, we perform successive Schmidt decompositions as shown diagrammatically in Fig. 3. We start by performing a Schmidt decomposition Eq. (1) of the state $|\psi\rangle$ into the first site and the rest such that

$$|\psi\rangle = \sum_{\alpha_1=1}^d A_{\alpha_1}^{[1]} |\alpha_1\rangle_{[1]} |\alpha_1\rangle_{[2, \dots, N]}. \quad (29)$$

The states $|\alpha_1\rangle_{[1]}$ and $|\alpha_1\rangle_{[2, \dots, N]}$ form an orthogonal basis for the left and right part, respectively. The first matrix $A_{\alpha_1}^{[1]j_1}$ in the MPS is the matrix relating the left Schmidt states $|\alpha_1\rangle_{[1]}$ with the local states $|j_1\rangle$ (describing the local states on the first site) and is given by $A_{\alpha_1}^{[1]j_1} = \langle j_1 | \alpha_1 \rangle_{[1]}$. The resulting mixed representation of the state reads

$$|\psi\rangle = \sum_{j_1=1}^d \sum_{\alpha_1=1}^d A_{\alpha_1}^{[1]j_1} A_{\alpha_1}^{[1]} |j_1\rangle |\alpha_1\rangle_{[2, \dots, N]}. \quad (30)$$

Next we proceed to the next bond and perform a Schmidt decomposition of the state such that

$$|\psi\rangle = \sum_{\alpha_2=1}^{d^2} A_{\alpha_2}^{[2]} |\alpha_2\rangle_{[1,2]} |\alpha_2\rangle_{[3, \dots, N]}. \quad (31)$$

The second matrix $A_{\alpha_1 \alpha_2}^{[2]j_2}$ then relates the mixed basis states $|\alpha_1\rangle_{[1]} |j_2\rangle$ with the left Schmidt states $|\alpha_2\rangle_{[1,2]}$ and is given by $A_{\alpha_1 \alpha_2}^{[2]j_2} = [\langle \alpha_1 |_{[1]} \langle j_2 |] |\alpha_2\rangle_{[1,2]}$. The resulting mixed representation of the state reads

$$|\psi\rangle = \sum_{\alpha_1=1}^d \sum_{\alpha_2=1}^{d^2} \sum_{j_1, j_2=1}^d A_{\alpha_1}^{[1]j_1} A_{\alpha_1 \alpha_2}^{[2]j_2} A_{\alpha_2}^{[2]} |j_1, j_2\rangle |\alpha_2\rangle_{[3, \dots, N]}. \quad (32)$$

This procedure can now be continued until reaching the right end of the chain. We choose the last matrix $A^{[N]j_N}$ to relate the states $\Lambda_{\alpha_N}|\alpha_N\rangle_{[N]}$ to the local basis $|j_N\rangle$. Then it is easy to see that we finally arrive at a representation of the state that has exactly the form Eq. (22).

Generically, the matrix dimension increases exponentially as we proceed toward the center of the chain. However, for area law states, we can make an approximation by neglecting the Schmidt states that have a very small Schmidt values. For the ground state of the Ising model discussed above, we can find a very good approximation of the ground state as MPS by keeping only a maximal bond dimension of ~ 20 with a truncation error that is of the order of the machine precision (independent of the system size).

3.3 Canonical form

The MPS representation Eq. (22) is not unique. Consider the bond between sites n and $n+1$, which defines a bipartition into $L = \{1, \dots, n\}$ and $R = \{n+1, \dots, N\}$. Given an invertible $\chi_{n+1} \times \chi_{n+1}$ matrix X , we can replace

$$M^{[n]j_n} \rightarrow \tilde{M}^{[n]j_n} := M^{[n]j_n} X^{-1}, \quad M^{[n+1]j_{n+1}} \rightarrow \tilde{M}^{[n+1]j_{n+1}} := X M^{[n+1]j_{n+1}} \quad (33)$$

and still represent the same state $|\psi\rangle$. This freedom can be used to define a convenient ‘‘canonical form’’ of the MPS, following Ref. [24, 25]. Without loss of generality, we can decompose the matrices $\tilde{M}^{[n]j_n} = \tilde{\Gamma}^{[n]j_n} \tilde{\Lambda}^{[n+1]}$, where $\tilde{\Lambda}^{[n+1]}$ is a square, diagonal matrix with positive entries $\tilde{\Lambda}_{\tilde{\alpha}_{n+1}}^{[n+1]}$ on the diagonal. Performing partial contractions gives a representation looking very similar to the Schmidt decomposition (1)

$$\begin{aligned} |\psi\rangle &= \sum_{j_1, \dots, j_N} M^{[1]j_1} \dots M^{[n-1]j_{n-1}} \tilde{\Gamma}^{[n]j_n} \tilde{\Lambda}^{[n+1]} \tilde{M}^{[n+1]j_{n+1}} M^{[n+2]j_{n+2}} \dots M^{[N]j_N} |j_1, \dots, j_N\rangle \\ &= \sum_{\tilde{\alpha}_{n+1}} \tilde{\Lambda}_{\tilde{\alpha}_{n+1}}^{[n+1]} |\tilde{\alpha}_{n+1}\rangle_L \otimes |\tilde{\alpha}_{n+1}\rangle_R, \quad \text{where} \end{aligned} \quad (34)$$

$$|\tilde{\alpha}_{n+1}\rangle_L = \sum_{j_1, \dots, j_n} \left(M^{[1]j_1} \dots M^{[n-1]j_{n-1}} \tilde{\Gamma}^{[n]j_n} \right)_{1, \tilde{\alpha}_{n+1}} |j_1, \dots, j_n\rangle, \quad (35)$$

$$|\tilde{\alpha}_{n+1}\rangle_R = \sum_{j_{n+1}, \dots, j_N} \left(\tilde{M}^{[n+1]j_{n+1}} M^{[n+2]j_{n+2}} \dots M^{[N]j_N} \right)_{\tilde{\alpha}_{n+1}, 1} |j_{n+1}, \dots, j_N\rangle. \quad (36)$$

However, for general M and $\tilde{\Gamma}^{[n]}$, the states $|\tilde{\alpha}_{n+1}\rangle_{L/R}$ will not be orthonormal. Note that we can interpret the X in Eq. (33) as a basis transformation of the states $|\tilde{\alpha}_{n+1}\rangle_R$ in Eq. (36). The idea of the canonical form is to choose the X in Eq. (33) such that it maps $|\tilde{\alpha}_{n+1}\rangle_R$ to the Schmidt states $|\alpha_{n+1}\rangle_R$. Using the Schmidt values $\Lambda_{\alpha_{n+1}}^{[n+1]}$ on the diagonal of $\tilde{\Lambda}^{[n+1]} \rightarrow \Lambda^{[n+1]}$, we find that Eq. (34) indeed gives the Schmidt decomposition. Repeating this on each bond yields the canonical form

$$|\Psi\rangle = \sum_{j_1, \dots, j_N} \Gamma^{[1]j_1} \Lambda^{[2]} \Gamma^{[2]j_2} \Lambda^{[3]} \dots \Lambda^{[N]} \Gamma^{[N]j_N} |j_1, \dots, j_N\rangle. \quad (37)$$

It turns out that the canonical form of MPS is extremely useful for different purposes. First, fixing the gauge degree of freedom allows for a more efficient optimization of MPS in numerical algorithms. Second, it provides convenient analytical properties for exactly proving certain universal properties, which we will use later on in the context of symmetry protected phases.

3.4 Time Evolving Block Decimation (TEBD)

Now that we know how to represent quantum states as MPS, we would like to manipulate them and use them for studying microscopic models. A very useful algorithm is the Time Evolving Block Decimation (TEBD) algorithm [26], which allows evaluating the time evolution of a MPS

$$|\psi(t)\rangle = U(t) |\psi(0)\rangle. \quad (38)$$

The time evolution operator U can either be $U(t) = \exp(-itH)$, yielding a real time evolution, or an imaginary time evolution $U(\tau) = \exp(-\tau H)$. The latter can be used to evaluate (finite temperature) Green functions or as a first, conceptually simple way to find the ground state of the Hamiltonian H through the relation

$$|\psi_{\text{GS}}\rangle = \lim_{\tau \rightarrow \infty} \frac{e^{-\tau H} |\psi_0\rangle}{\|e^{-\tau H} |\psi_0\rangle\|}. \quad (39)$$

The TEBD algorithm makes use of the Suzuki-Trotter decomposition [27], which approximates the exponent of a sum of operators with a product of exponents of the same operators. For example, the first and second order expansions read

$$e^{(X+Y)\delta} = e^{X\delta} e^{Y\delta} + \mathcal{O}(\delta^2), \quad (40)$$

$$e^{(X+Y)\delta} = e^{X\delta/2} e^{Y\delta} e^{X\delta/2} + \mathcal{O}(\delta^3). \quad (41)$$

Here X and Y are operators, and δ is a small parameter. To make use of these expressions, we assume that the Hamiltonian is a sum of two-site operators of the form $H = \sum_n h^{[n,n+1]}$, where $h^{[n,n+1]}$ acts only on sites n and $n+1$, and decompose it as a sum

$$H = \underbrace{\sum_{n \text{ odd}} h^{[n,n+1]}}_{H_{\text{odd}}} + \underbrace{\sum_{n \text{ even}} h^{[n,n+1]}}_{H_{\text{even}}}. \quad (42)$$

Each term H_{odd} and H_{even} consists of a sum of commuting operators, therefore $e^{H_{\text{odd}}\delta} = \prod_{n \text{ odd}} e^{h^{[n,n+1]}\delta}$ and similar for H_{even} . We now divide the time into small time slices $\delta t \ll 1$ (the relevant time scale is in fact the inverse gap) and consider a time evolution operator $U(\delta t)$. Using, as an example, in the first order decomposition (40), the operator $U(\delta t)$ can be expanded into products of two-site unitary operators

$$U(\delta t) \approx \left[\prod_{n \text{ odd}} U^{[n,n+1]}(\delta t) \right] \left[\prod_{n \text{ even}} U^{[n,n+1]}(\delta t) \right], \quad (43)$$

where $U^{[n,n+1]}(\delta t) = e^{-i\delta t h^{[n,n+1]}}$. The successive application of these two-site unitary operators to an MPS is the main part of the algorithm and explained in the following.

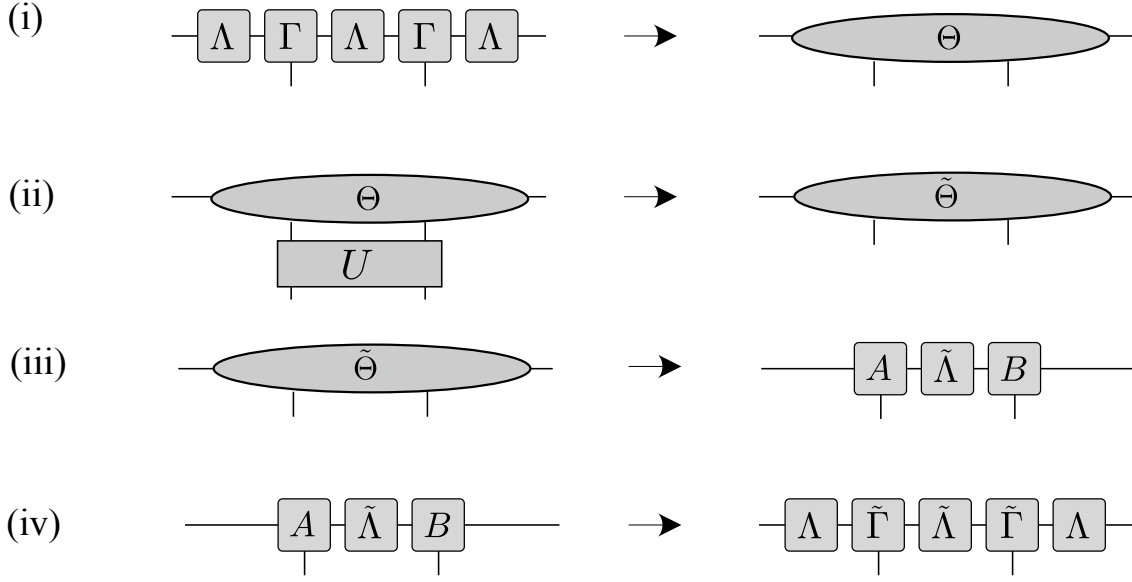


Fig. 4: Update to apply a two-site unitary U and recover the canonical MPS form (see text for details). Note that we do not explicitly label the positions of the individual tensors in favor for a less cluttered presentation.

Local unitary updates of an MPS. One of the advantages of the MPS representation is that local transformations can be performed efficiently. Moreover, the canonical form discussed above is preserved if the transformations are unitary [24].

A one-site unitary U simply transforms the tensors Γ of the MPS

$$\tilde{\Gamma}_{\alpha_n \alpha_{n+1}}^{[n] j_n} = \sum_{j'_n} U_{j'_n}^{j_n} \Gamma_{\alpha_n \alpha_{n+1}}^{[n] j'_n}. \quad (44)$$

In such a case the entanglement of the wave-function is not affected and thus the values of Λ do not change. The update procedure for a two-site unitary transformation acting on two neighboring sites n and $n + 1$ is shown in Fig. 4. We first find the wave function in the basis spanned by the left Schmidt states $|\alpha_n\rangle_L$, the local basis $|j_n\rangle$ and $|j_{n+1}\rangle$ on sites n and $n + 1$, and the right Schmidt states $|\alpha_{n+2}\rangle_R$, which together form an orthonormal basis $\{ |\alpha_n\rangle_L \otimes |j_n\rangle \otimes |j_{n+1}\rangle \otimes |\alpha_{n+2}\rangle_R \}$. Calling the wave function coefficients Θ , the state is expressed in a mixed bases as

$$|\psi\rangle = \sum_{\alpha_n, j_n, j_{n+1}, \alpha_{n+2}} \Theta_{\alpha_n \alpha_{n+2}}^{j_n j_{n+1}} |\alpha_n\rangle_L |j_n\rangle |j_{n+1}\rangle |\alpha_{n+2}\rangle_R. \quad (45)$$

Using the definitions of the canonical form, Θ is given by

$$\Theta_{\alpha_n \alpha_{n+2}}^{j_n j_{n+1}} = \sum_{\alpha_{n+1}} \Lambda_{\alpha_n}^{[n]} \Gamma_{\alpha_n \alpha_{n+1}}^{[n], j_n} \Lambda_{\alpha_{n+1}}^{[n+1]} \Gamma_{\alpha_{n+1} \alpha_{n+2}}^{[n+1], j_{n+1}} \Lambda_{\alpha_{n+2}}^{[n+2]}. \quad (46)$$

Writing the wave function in this basis is useful because it is easy to apply the two-site unitary in step (ii) of the algorithm

$$\tilde{\Theta}_{\alpha_n \alpha_{n+2}}^{j_n j_{n+1}} = \sum_{j'_n j'_{n+1}} U_{j'_n j'_{n+1}}^{j_n j_{n+1}} \Theta_{\alpha_n \alpha_{n+2}}^{j'_n j'_{n+1}}. \quad (47)$$

Next we have to extract the new tensors $\tilde{B}^{[n]}$, $\tilde{B}^{[n+1]}$ and $\tilde{\Lambda}^{[n+1]}$ from the transformed tensor $\tilde{\Theta}$ in a manner that preserves the canonical form. We first “reshape” the tensor $\tilde{\Theta}$ by combining indices to obtain a $d\chi_n \times d\chi_{n+2}$ dimensional matrix $\tilde{\Theta}_{j_n \alpha_n; j_{n+1} \alpha_{n+2}}$. Because the basis $\{ |\alpha_n\rangle_L \otimes |j_n\rangle \}$ is orthonormal, as for the right, it is natural to decompose the matrix using the singular value decomposition (SVD) in step (iii) into

$$\tilde{\Theta}_{j_n \alpha_n; j_{n+1} \alpha_{n+2}} = \sum_{\alpha_{n+1}} \tilde{A}_{j_n \alpha_n; \alpha_{n+1}}^{[n]} \tilde{\Lambda}_{\alpha_{n+1} \alpha_{n+1}}^{[n+1]} \tilde{B}_{\alpha_{n+1}; j_{n+1} \alpha_{n+2}}^{[n+1]}, \quad (48)$$

where $\tilde{A}^{[n]}$, $\tilde{B}^{[n+1]}$ are isometries and $\tilde{\Lambda}^{[n+1]}$ is a diagonal matrix. Indeed, the suggestive notation that the new tensors are in mixed canonical form is justified, since the SVD yields a Schmidt decomposition of the wave function for a bipartition at the bond between sites n and $n+1$. The isometry $\tilde{A}^{[n]}$ relates the new Schmidt states $|\alpha_{n+1}\rangle_L$ to the combined bases $|\alpha_n\rangle_L \otimes |j_n\rangle$. Analogously, the Schmidt states for the right site are obtained from the matrix $\tilde{B}^{[n+1]}$. Thus the diagonal matrix $\tilde{\Lambda}^{[n+1]}$ contains precisely the Schmidt values of the transformed state. In a last step (iv), we reshape the obtained matrices $\tilde{A}^{[n]}$, $\tilde{B}^{[n+1]}$ back to tensors with 3 indices and recover the right canonical form by

$$\tilde{\Gamma}_{\alpha_n \alpha_{n+1}}^{[n] j_n} = (\Lambda^{[n]})_{\alpha_n}^{-1} \tilde{A}_{j_n \alpha_n; \alpha_{n+1}}^{[n]} \quad \text{and} \quad \tilde{\Gamma}_{\alpha_{n+1} \alpha_{n+2}}^{[n+1] j_{n+1}} = \tilde{B}_{\alpha_{n+1}; j_{n+1} \alpha_{n+2}}^{[n+1]} (\Lambda^{[n+2]})_{\alpha_{n+2}}^{-1}. \quad (49)$$

After the update, the new MPS is still in the canonical form. The entanglement at the bond between n and $n+1$ has changed and the bond dimension increased to $d\chi$. Thus the amount of information in the wave function grows exponentially if we successively apply unitaries to the state. To overcome this problem, we perform an approximation by fixing the maximal number of Schmidt terms to χ_{\max} . In each update, only the χ_{\max} most important states are kept in step (iii), i.e., if we order the Schmidt states according to their size we simply truncate the range of the index α_{n+1} in Eq. (48) to be $1 \dots \chi_{\max}$. This approximation limits the dimension of the MPS and the tensors B have at most a dimension of $\chi_{\max} \times d \times \chi_{\max}$. Given that the truncated weight is small, the normalization conditions for the canonical form will be fulfilled to a good approximation. In order to keep the wave function normalized, one should divide by the norm after the truncation, i.e., divide by $\mathcal{N} = \sqrt{\sum_{j_n, j_{n+1}, \alpha_n, \alpha_{n+2}} |\Theta_{\alpha_n \alpha_{n+2}}^{j_n j_{n+1}}|^2}$.

Using the TEBD algorithm, we can now perform real and imaginary time evolution of MPS. While the imaginary time evolution provides a tool to find ground states, it turns out that a variational optimization is often more efficient. This is done using the density-matrix renormalization group (DMRG) method [28]. The DMRG replaces step (ii) in the TEBD algorithm, in which the two site gate is applied, with a variational optimization of the local tensors. This can be done using for example the Lanczos algorithm. Instead we refer to the existing literature for further details [4, 5].

4 Symmetry-protected topological (SPT) phases

Symmetry and topology are cornerstones in the characterization of quantum phases of matter. The classification of phases in terms of spontaneously broken symmetries is well known, for example the ferro- and paramagnetic phase of the transverse field Ising model. Topological phases of matter are more subtle and require new frameworks for their theoretical understanding.

We consider a gapped one-dimensional system with bosonic degrees of freedom of length L that is invariant under a global symmetry group G . An example of such symmetry is the \mathbb{Z}_2 symmetry $\bigotimes_j \sigma_j^x$ of the transverse field Ising model Eq. (10). Note that the classification scheme needs the symmetries to be well-defined even when having open boundaries, which for a unitary symmetry $\bigotimes_j u_j(g)$ with $g \in G$ is guaranteed if it is a product over local symmetry operations $u_j(g)$ on sites (or unit cells), referred to as an on-site symmetry. More general symmetries (such as for example spatial inversion symmetry) will require a more general “entanglement based” approach which we will discuss below. If we assume that the symmetry is not spontaneously broken, then for periodic boundary conditions the ground state must be unique and hence invariant, i.e.,

$$|\psi\rangle = \left[\bigotimes_n u_n(g) \right] |\psi\rangle. \quad (50)$$

However, if we have open boundary conditions, then the absence of spontaneous symmetry breaking in the bulk still allows for the symmetry operation to act non-trivially near the edges. Since the bulk is invariant and thus not affected by the symmetry operation, we can formally write this as $\bigotimes_j u_j(g) = U_L(g)U_R(g)$ —which is valid in the ground state subspace. These effective operators U_L and U_R are exponentially localized near the boundaries on a length-scale set by the correlation length. In the thermodynamic limit ($L \rightarrow \infty$) $U_L(g)$ and $U_R(g)$ have no overlap and since the Hamiltonian is local, this means that $U_L(g)$ and $U_R(g)$ do not change the energy of a state in the ground state subspace. We refer to this as symmetry fractionalization. The same holds for any other unbroken symmetry $h \in G$, so we can equivalently write $U_L(h)U_R(h)$. Any group relation between g and h then implies a relation between the edge symmetries. In particular, $\{U_L(g), U_L(h), \dots\}$ then obey the same group relations as G , possibly up to a phase factor. In the bosonic case, where U_L and U_R commute, both edges completely decouple and the physical symmetry is then *projectively* represented on each edge (see next section for details about projective representations). Such a projective representation has discrete labels that cannot change smoothly. Since any non-trivial projective representation has a minimal dimension > 1 , it protects degenerate modes on the edge.

4.1 Projective representations

Let us consider a group G with group elements $g_i \in G$ and discuss how to classify different SPT phases. The matrices $U(g_i)$ form a *projective* representation of G if

$$U(g_i)U(g_j) = \omega(g_i, g_j)U(g_i g_j), \quad (51)$$

where $\omega(g_i, g_j) \in U(1)$ represent the so-called *factor set*. Thus a projective representation is a linear representation modulo a $U(1)$ phase factor. In the case that all phase factors are unity, the representation is a linear representation of the group. Because of the associativity of the group, i.e., the elements of G fulfill $g_i(g_j g_k) = (g_i g_j)g_k$, the factor set must satisfy

$$\omega(g_j, g_k)\omega(g_i, g_j g_k) = \omega(g_i g_j)\omega(g_i g_j, g_k). \quad (52)$$

Transforming the matrices as $\tilde{U}(g_i) = \beta(g_i)U(g_i)$, $\beta(g_i) \in U(1)$ yields a new factor set

$$\tilde{\omega}(g_i, g_j) = \frac{\beta(g_i g_j)}{\beta(g_i)\beta(g_j)}\omega(g_i, g_j). \quad (53)$$

Two projective representations $\tilde{U}(g)$ and $U(g)$ that are related by such a transformation are considered to be equivalent and belong to the same class.

It was Isaac Schur who derived in 1904 a classification of different types of projective representation using so called ‘‘Schur multipliers’’ to label different classes. These correspond to the second cohomology group $H_2(G, U(1))$ of a group G . Instead of discussing the details of the proof, we refer for a general introduction to Ref. [29] and consider some simple examples.

(1) Group \mathbb{Z}_N . The generators of the group are $\exp(i\pi/N)$ rotations and the group elements are $\{1, R, R^2, \dots, R^N\}$. For a projective representation of the group we can assign an arbitrary phase such that $U^N(R) = \exp(i\varphi)$. However, a simple rescaling $U(R)$ by $\exp(i\varphi/N)$ can always transform the projective representation to a linear one. Thus this group has only one class and all projective representation can be transformed into a linear one.

(2) Group $\mathbb{Z}_2 \times \mathbb{Z}_2$. This group is generated by π rotations R_x and R_z about two orthogonal axes. Clearly, $R_x^2 = R_z^2 = 1$ and $R_z R_x = R_x R_z$, thus the group elements are $\{1, R_x, R_z, R_x R_z\}$. The group $\mathbb{Z}_2 \times \mathbb{Z}_2$ has two different classes of projective representations which can be distinguished by the gauge invariant phase factor

$$U(R_x)U(R_z)U^{-1}(R_x)U^{-1}(R_z) = \exp(i\varphi)$$

with $\varphi = 0, \pi$. Clearly, as each element occurs with its inverse, the phase of the commutator cannot be change by rephasing the operators.

Both cases can be realized using a representation of the rotations in terms of spin operators by $U(R_x) = \exp(i\pi S^x)$ and $U(R_z) = \exp(i\pi S^z)$. The $S = 1$ representation with

$$S^x = \frac{1}{\sqrt{2}} \begin{pmatrix} 0 & 1 & 0 \\ 1 & 0 & 1 \\ 0 & 1 & 0 \end{pmatrix}, \quad S^z = \begin{pmatrix} -1 & 0 & 0 \\ 0 & 0 & 0 \\ 0 & 0 & 1 \end{pmatrix}. \quad (54)$$

is a linear ($\varphi = 0$) representation. The $S = 1/2$ spin matrices

$$S^x = \frac{1}{2} \begin{pmatrix} 0 & 1 \\ 1 & 0 \end{pmatrix}, \quad S^z = \frac{1}{2} \begin{pmatrix} 1 & 0 \\ 0 & -1 \end{pmatrix}. \quad (55)$$

form a projective ($\varphi = \pi$) representation. This can be seen easily as $U(R_x) = \sigma_x$ and $U(R_z) = \sigma_z$ anti-commute (σ_x, σ_z are the Pauli matrices).

4.2 MPS representations of SPT phases

For the study of SPT phases, it will be useful to derive how symmetry operations act on MPS in the canonical form. Let us consider an on-site symmetry operation which is applied to all sites

$$|\tilde{\psi}\rangle = \left[\bigotimes_n u_n(g) \right] |\psi\rangle, \quad (56)$$

where $u_n(g)$ is acting on site n with g being an element of the symmetry group G under which the state $|\psi\rangle$ is invariant. In the MPS formulation, the transformation corresponds to contracting the symmetry operation with all physical legs as shown in Fig. 5(a). In Ref. [30] it was shown that for an MPS in canonical form the matrices Γ^j transform under symmetry operations g as

$$\sum_{j'} u_{jj'}(g) \Gamma^{j'} = e^{i\theta(g)} U^\dagger(g) \Gamma^j U(g), \quad (57)$$

with a diagrammatic representation as shown in Fig. 5(b). Here $U(g)$ is a unitary matrix which commutes with the Λ matrices, and $e^{i\theta(g)}$ is a phase.² It is clear that this is a sufficient condition for the MPS to be symmetric. To show that it is a necessary condition, one has to apply the Schwarz inequality and use conditions of the canonical form [30].

Equivalently to the discussion above, it can be shown that the matrices $U(g)$ form a χ -dimensional *linear* or *projective* representation of the symmetry group of the wave function and $e^{i\theta(g)}$ is a linear (1D) representation [6]. The matrices $U(g)$ are actually a representation of the symmetry operations in the basis of Schmidt states (this can be seen by going back to the definition of the canonical form). Note that we assumed a translationally invariant MPS but we can directly generalize the concept to the general case by allowing site dependent $U(g)$.

Similar relations can be derived for symmetries that are not on-site operations. For a time reversal transformation Γ^j is transformed to $(\Gamma^j)^*$ (complex conjugate) on the left hand side (including possible spin rotations). In the case of inversion symmetry Γ^j is transformed to $(\Gamma^j)^T$ (transpose) on the left hand side of Eq. (57). We refer to Refs. [6, 7] for further details.

4.3 Simple examples of different SPT phases

We will now consider two different MPSs for a spin-1 chain that belong to different symmetry protected phases protected by the $\mathbb{Z}_2 \times \mathbb{Z}_2$ symmetry, i.e, π rotations about the x and z axis. Clearly, the onsite representation of the $\mathbb{Z}_2 \times \mathbb{Z}_2$ in terms of the $S = 1$ degrees of freedom is a linear one. Let us now analyze how the MPS representation of two different states transforms under the $\mathbb{Z}_2 \times \mathbb{Z}_2$ symmetry.

Spin-1 AKLT state: The AKLT state has $SO(3)$ symmetry and $\mathbb{Z}_2 \times \mathbb{Z}_2$ is a subgroup thereof. Since the MPS representation Eq. (28) is very simple, we can directly extract the projective representation by applying the symmetry operations and find that

$$U(R_x) = \sigma_x, \quad U(R_z) = \sigma_z$$

²As $U(g)$ commutes with Λ , it also commutes with the reduced density matrices ρ^L and ρ^R .

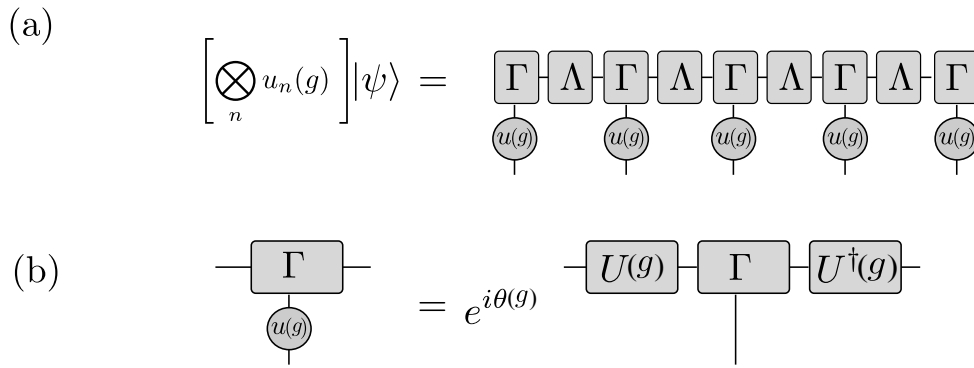


Fig. 5: (a): Transformation of an MPS under an on-site symmetry g applied to all sites. (b): Representation of a symmetry operation in terms of the MPS.

and $\theta = \pi$ (To arrive at this result, one can simply apply the on-site symmetry operations to the MPS). The representation of $\mathbb{Z}_2 \times \mathbb{Z}_2$ is a projective one with the gauge invariant phase factor $U(R_x)U(R_z)U^\dagger(R_x)U^\dagger(R_z) = -1$.

Spin-1 product state: A product state of $S^z = 0$ eigenstates of the form $|0\rangle \otimes |0\rangle \otimes \cdots \otimes |0\rangle$ is invariant under $\mathbb{Z}_2 \times \mathbb{Z}_2$ and the MPS transforms trivially under $\mathbb{Z}_2 \times \mathbb{Z}_2$ rotations

$$U(R_x) = 1, U(R_z) = 1$$

with $U(R_x)U(R_z)U^\dagger(R_x)U^\dagger(R_z) = 1$ and $\theta = 0$.

As argued above, these phase factors characterize the two phases as they cannot be changed unless the symmetry is broken or the system undergoes a phase transition. Thus we have identified two representatives of different SPT phases.

4.4 Degeneracies in the entanglement spectrum

Here we discuss some practical ideas of how to detect SPT in numerical simulations in terms of the entanglement spectrum. Topological phases with non-trivial projective representations necessarily have degeneracies in the entanglement spectrum. That is, *all* eigenvalues of the reduced density matrices ρ^L and ρ^R for the bipartition of the system into two half-chains are degenerate.

To see this, let us assume that the ground state is represented as a MPS and is symmetric under a symmetry group G . Using the Eq. (57), we find the symmetry representation $U(g)$ in terms of the auxiliary indices which commutes with the reduced density matrices. If the $U(g)$ for $g \in G$ form a projective representation of the symmetry group, we can find a set of non-commuting elements such that for example $U(g_i)U(g_j)U(g_i)^\dagger U(g_j)^\dagger = \exp(i\varphi)$. The non-trivial commutation relations require that the irreducible representations have dimensions larger than one, which yields degeneracies in the spectrum of ρ^L and (ρ^R) . For example, if $\varphi = \pi$, the spectrum is doubly degenerate, since ρ^L and ρ^R commute with the two unitary matrices U_x, U_z which anti-commute among themselves.

5 Universal entanglement scaling at critical points

In the previous section, we mainly focused on local and gapped Hamiltonians for which we found an area law. We will now shift our attention to ground states at critical points where the correlation length diverges and the state becomes scale invariant. The microscopic details become irrelevant for the long wavelength physics and according to the universality hypothesis, certain quantities only depend on basic properties like the symmetry of the system.

Many critical points in one-dimensional systems can be described by *conformal field theories* (CFT). A CFT is a quantum field theory that is invariant under conformal transformations (i.e., transformations that locally preserve angles, but not necessarily lengths). The number of independent conformal transformations is infinite for 1+1D, which makes conformal symmetry highly constraining in this case. As a result, conformally invariant critical points in 1+1 dimensions can be described by a small number of parameters. One of the key quantities in this context is the *central charge* c , which is a universal quantity that quantifies the low energy degrees of freedom of the theory. For example, for free bosons $c = 1$, whereas the Ising universality class has $c = 1/2$.

We will now show that the central charge is intimately linked to the bipartite entanglement entropy [9,8]. Let us compute the entanglement entropy for the bipartition of a 1+1 dimensional lattice model from the reduced density matrix ρ_A . Since the eigenvalues lie in the interval $[0, 1]$ and $\text{Tr} \rho_A = 1$, $\text{Tr} \rho_A^n$ is convergent and analytic for all $\text{Re } n > 1$. Hence we can obtain the entanglement entropy using

$$S = - \lim_{n \rightarrow 1} \frac{\partial}{\partial n} \text{Tr} \rho_A^n. \quad (58)$$

While calculating $\text{Tr} \rho_A^n$ for a generic n is not feasible, it is possible for positive integer n using the replica trick and then analytically continuing it to a general complex value. In particular, the calculation for positive integer n reduces to that of a partition function on a Riemann surface that is analytically achievable in a quantum field theory. Using this approach, it is now possible to obtain the entanglement entropy for a 1+1 dimensional CFT in different settings:

First, we consider the case in which we cut out ℓ consecutive sites from an infinite chain for which we find [9]

$$S = \frac{c}{3} \log \left(\frac{\ell}{a} \right) + \mathcal{O}(1). \quad (59)$$

Here c is the central charge and a is an ultraviolet cutoff, corresponding to a lattice spacing. Thus the entanglement entropy does not exhibit an area law but instead diverges logarithmically. Moreover, the Rényi entropies are given by

$$S_n = \frac{c}{6} \left(1 + \frac{1}{n} \right) \log \left(\frac{\ell}{a} \right) + \mathcal{O}(1). \quad (60)$$

Second, we consider the case in which we cut a finite chain of length L into two pieces of length ℓ and $L - \ell$ for which we obtain

$$S = \frac{c}{6} \log \left(\frac{2L}{\pi a} \sin \frac{\pi \ell}{L} \right) + \mathcal{O}(1), \quad (61)$$

with the special case for a bipartition into two equally sized halves,

$$S = \frac{c}{6} \log \left(\frac{\ell}{a} \right) + \mathcal{O}(1). \quad (62)$$

The coefficient in front of the logarithm is thus half of the one where we cut out a finite block from an infinite system. These above two formulas are particularly useful for extracting the central charge from finite size numerics.

Third, we consider an infinite system that is close to a critical point, where the correlation length is large but finite. In this case one can often still effectively describe the system by a conformal field theory. One then obtains for the entanglement entropy [31]

$$S = \frac{c}{6} \log \left(\frac{\xi}{a} \right) + \mathcal{O}(1). \quad (63)$$

The latter formula is very useful for infinite-system MPS based simulations of critical points, where a finite bond dimension induces a finite correlation length. In this *entanglement scaling* approach, a simulation at the critical point is performed with increasing bond dimension, which can be used to extract the central charge [32, 33].

6 Case study: Phase diagram of a spin-1 chain

We now demonstrate the usefulness of the entanglement based quantities we derived in the preceding sections to numerically study the phase diagram of a spin-1 chain. For this we will first use MPS based methods to obtain the ground state and then analyze its properties using entanglement spectroscopy and entanglement scaling.

We will investigate the phase diagram of the Hamiltonian

$$H = J \sum_j \vec{S}_j \cdot \vec{S}_{j+1} + D \sum_j (S_j^z)^2, \quad (64)$$

where the first term is the spin-1 Heisenberg coupling ($J > 0$) and the second term is a single ion anisotropy ($D > 0$). This model has various symmetries that can protect SPT phases, including time reversal, inversion symmetry, and $\mathbb{Z}_2 \times \mathbb{Z}_2$ spin rotation symmetry. The phase diagram of this model is well known (Ref. [34] and citations therein) and thus it serves as a good testing case.

In order to understand the phase diagram, let us first consider the limiting cases:

- For $D \ll J$, the model reduces to the antiferromagnetic spin-1 Heisenberg model and the ground state is in the Haldane phase [35], which also contains the AKLT state $|\psi_{\text{AKLT}}\rangle$ [21]. Based on the consideration made in Section 4, we know that the ground state is in a non-trivial SPT phase.
- For $D \gg J$, the ground state is adiabatically connected to a simple product state $|\psi_{\text{large } D}\rangle = |0\rangle \otimes |0\rangle \otimes \cdots \otimes |0\rangle$, which is thus in a trivial phase.

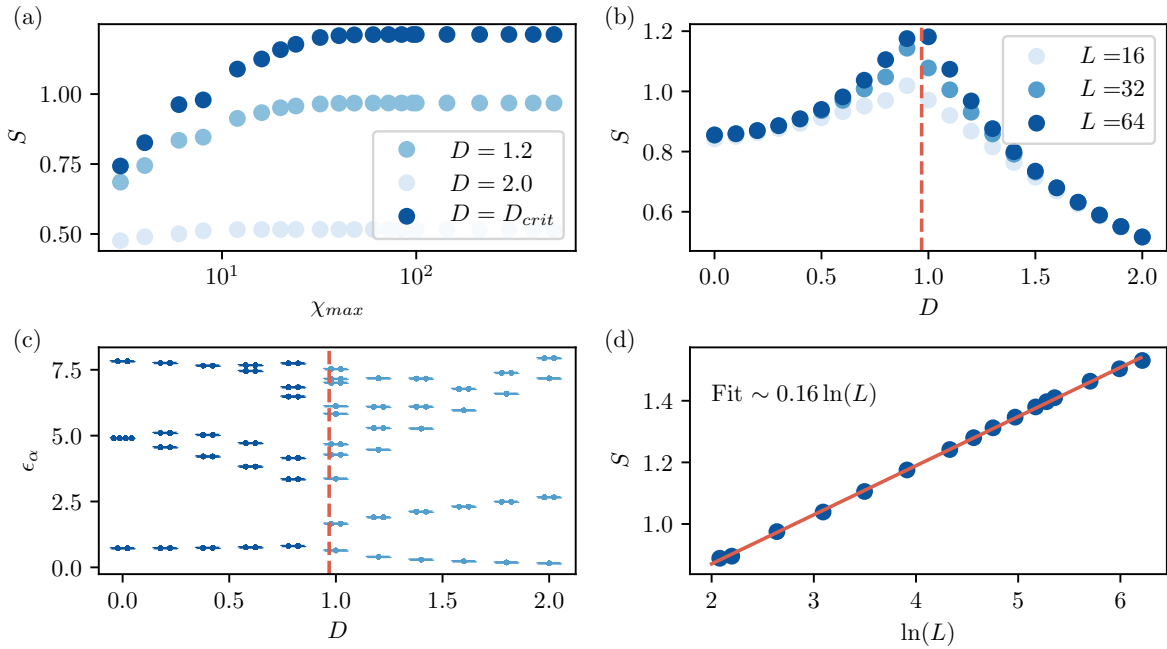


Fig. 6: (a) Half-chain entanglement entropy for the spin-1 chain Eq. (64) of length $L = 128$ as function of the bond dimension χ_{\max} used for the MPS simulations for different D . (b) Half-chain entanglement entropy for different systems sizes as function of D . The dashed line indicates the location of the exact critical point [34]. (c) Entanglement spectrum as function of D with a characteristic degeneracy in the Haldane phase. (d) Scaling of the entanglement entropy at the critical point, allowing us to extract a central charge $c = 1$.

Consequently, there has to be a phase transition between the two limiting cases.

We use the DMRG [28] method to variationally optimize an MPS ansatz for the ground state of the Hamiltonian and implement the code in Python with the TeNpy package [5]. A minimal code that finds the MPS representation for a spin-1 chain reads:

```
from tenpy.networks.mps import MPS
from tenpy.models.spins import SpinModel
from tenpy.algorithms import dmrg

M = SpinModel({"S":1, "L": 16, "bc_MPS": "finite",
              "Jx": 0, "Jy": 0, "Jz": 0, "D":2})
psi = MPS.from_product_state(M.lat.mps_sites(), [1]*16, "finite")
dmrg_params = {"trunc_params": {"chi_max": 30, "svd_min": 1.e-10}}
info = dmrg.run(psi, M, dmrg_params)
print("S[j] =", psi.entanglement_entropy())
```

For numerical stability, we add a small field at the first and last site to prevent the edge modes from coupling to each other. To test the convergence and figure out the required bond dimension χ_{\max} , we plot the half-chain entanglement entropy S in Fig. 6(a). We find that S converges for relatively small χ_{\max} for the system sizes considered. Indeed, based on the area law, we expect that the required bond dimension is independent of system size in gapped phases. However, the

entanglement entropy diverges logarithmically at critical points and thus the bond dimension has to be increased as we increase the system size (typically $\chi_{\max} \sim L^\kappa$ for some model specific exponent $\kappa > 0$). The logarithmic divergence of the entanglement entropy provides a useful signature to determine critical points in phase diagrams as seen in Fig. 6(b). We can clearly distinguish the area law behavior in the gapped phases from the critical point. Similar techniques have been used in the literature to pinpoint the critical point at $D_C/J = 0.96845(8)$ [34]. The entanglement spectrum shown in Fig. 6(c) shows the characteristic degeneracy throughout the Haldane phase and only accidental degeneracies in the large D phase. Note that we could also use non-local order parameters to distinguish the two phases [36, 37]. Lastly we focus on the properties of the critical point and investigate the entanglement scaling in Fig. 6(d). Using Eq. (62), we extract a central charge of $c = 1$, compatible with the universality of a Gaussian transition [38].

The tools applied in this case study can (in principle) be applied to determine the phase diagram of any one-dimensional model Hamiltonian. The main obstacle is that the ground state might be highly entangled, preventing an accurate representation as an MPS. This is particularly the case when considering critical phases, especially if the central charge is large.

7 Conclusions and further developments

In these lecture notes, we discussed a few aspects of many-body entanglement. After a general introduction, we introduced the *area law* which is commonly obeyed by ground states of local Hamiltonians, i.e., the leading term of the entanglement entropy grows at most proportionally with the boundary between the two partitions. This is in contrast to the *volume law* which is found for random or highly excited states. The area law and resulting locality of the ground state are extremely helpful to investigate the intricate structure of quantum many-body states and their emergent quantum orders. To demonstrate this, we focused on three different applications to one-dimensional quantum spin systems: First, we showed that area law states can be efficiently represented using MPSs—which are the basis for several algorithms that allow to simulate large quantum systems. Second, we investigated the entanglement properties of ground states and how they transform under symmetries, providing a framework for the classification of SPT phases. Third, we identified universal scaling properties of the entanglement entropies.

We obviously only covered a small fraction of this fast moving and rich field. Let us close by briefly mentioning some exciting aspects that could not be covered in these notes.

Topological entanglement. The entanglement entropy for a simply connected region for a two-dimensional system has the general form $S = \alpha|\partial A| - \gamma + \dots$, where α in the leading term is a non-universal coefficient and $|\partial A|$ is the perimeter of the subsystem. The sub-leading term γ , also known as the topological entanglement entropy, is universal and reflects the anyonic content that characterizes the topological order [39, 40]. This is directly related to the total quantum dimension (D) of the underlying topological field theory as $\gamma = \log D$. The topological entanglement is a very useful quantity to detect topological orders.

Many-body localization. So far we only discussed entanglement of ground states but the concept is also very useful to characterize non-equilibrium properties. One of the most remarkable predictions of quantum mechanics is that an arbitrarily weak random potential is sufficient to localize all energy eigenstates of a single particle moving in one dimension. Recent work has proposed that, if there are electron-electron interactions but the electronic system is isolated from other degrees of freedom, there can be a many-body localization (MBL) transition even in a one-dimensional system for which all the single-particle states are localized [41]. Entanglement is useful to characterize MBL in different ways: First, while the highly excited eigenstates of generic Hamiltonians fulfill a volume law, the eigenstates of a fully MBL systems obey an area law [42]. Thus the entanglement of eigenstates serves as an “order parameter” to detect a transition from an extended to an MBL phase. Second, the dynamical properties of the entanglement entropy allow us to distinguish a non-interacting (Anderson) localized system from an MBL system. While the entanglement following a quantum quench saturates for the former, it shows a logarithmic growth as function of time for the latter [43].

Acknowledgement.

We would like to acknowledge Rohit Dilip for performing the DMRG simulations presented in the case study and for useful comments on the manuscript. We also want to thank Johannes Hauschild for coauthoring related lecture notes on tensor-network simulations [5] that are partly reproduced in the matrix-product state section.

References

- [1] E. Schrödinger, Proceedings of the Cambridge Philosophical Society **31**, 555 (1935)
- [2] A. Einstein, B. Podolsky, and N. Rosen, Phys. Rev. **47**, 777 (1935)
- [3] J. Eisert, M. Cramer, and M.B. Plenio, Rev. Mod. Phys. **82**, 277 (2010)
- [4] U. Schollwöck, Ann. Phys. (N. Y). **326**, 96 (2011)
- [5] J. Hauschild and F. Pollmann, SciPost Phys. Lect. Notes p. 5 (2018)
- [6] F. Pollmann, A.M. Turner, E. Berg, and M. Oshikawa, Phys. Rev. B **81**, 064439 (2010)
- [7] X. Chen, Z.-C. Gu, and X.-G. Wen, Phys. Rev. B **83**, 035107 (2011)
- [8] P. Calabrese and J. Cardy, J. Phys. A: Mathematical and Theoretical **42**, 504005 (2009)
- [9] C. Holzhey, F. Larsen, and F. Wilczek, Nuclear Physics B **424**, 443 (1994)
- [10] M.B. Hastings, I. González, A.B. Kallin, and R.G. Melko, Phys. Rev. Lett. **104**, 157201 (2010)
- [11] A. Elben, B. Vermersch, M. Dalmonte, J.I. Cirac, and P. Zoller, Phys. Rev. Lett. **120**, 050406 (2018)
- [12] D.A. Abanin and E. Demler, Phys. Rev. Lett. **109**, 020504 (2012)
- [13] H. Li and F.D.M. Haldane, Phys. Rev. Lett. **101**, 010504 (2008)
- [14] D.N. Page, Phys. Rev. Lett. **71**, 1291 (1993)
- [15] M.B. Hastings, J. Stat. Mech. Theory Exp. **2007**, P08024 (2007)
- [16] I. Peschel and M.-C. Chung, J. Phys. A: Mathematical and General **32**, 8419 (1999)
- [17] I. Peschel, Journal of Physics A: Mathematical and General **36**, L205 (2003)
- [18] M. Fannes, B. Nachtergaele, and R.F. Werner, Commun. Math. Phys. **144**, 443 (1992)
- [19] S. Östlund and S. Rommer, Phys. Rev. Lett. **75**, 3537 (1995)
- [20] S. Rommer and S. Östlund, Phys. Rev. B **55**, 2164 (1997)
- [21] I. Affleck, T. Kennedy, E.H. Lieb, and H. Tasaki, Phys. Rev. Lett. **59**, 799 (1987)
- [22] D. Gottesman and M.B. Hastings, New J. Phys. **12**, 025002 (2010)
- [23] N. Schuch, M.M. Wolf, F. Verstraete, and J.I. Cirac, Phys. Rev. Lett. **100**, 030504 (2008)
- [24] G. Vidal, J.I. Latorre, E. Rico, and A. Kitaev, Phys. Rev. Lett. **90**, 227902 (2003)

- [25] G. Vidal, Phys. Rev. Lett. **98**, 070201 (2007)
- [26] G. Vidal, Phys. Rev. Lett. **93**, 040502 (2004)
- [27] M. Suzuki, J. Math. Phys. **32**, 400 (1991)
- [28] S.R. White, Phys. Rev. Lett. **69**, 2863 (1992)
- [29] G. Karpilovsky: *The Schur multiplier*. LMS monographs (Clarendon Press, 1987)
- [30] D. Perez-Garcia, M.M. Wolf, M. Sanz, F. Verstraete, and J.I. Cirac, Phys. Rev. Lett. **100**, 167202 (2008)
- [31] P. Calabrese and J. Cardy, J. Stat. Mech. **2004**, P06002 (2004)
- [32] L. Tagliacozzo, T.R. de Oliveira, S. Iblisdir, and J.I. Latorre, Phys. Rev. B **78**, 024410 (2008)
- [33] F. Pollmann, S. Mukerjee, A.M. Turner, and J.E. Moore, Phys. Rev. Lett. **102**, 255701 (2009)
- [34] S. Hu, B. Normand, X. Wang, and L. Yu, Phys. Rev. B **84**, 220402 (2011)
- [35] F.D.M. Haldane, Phys. Lett. A **93**, 464 (1983)
- [36] M. den Nijs and K. Rommelse, Phys. Rev. B **40**, 4709 (1989)
- [37] F. Pollmann and A.M. Turner, Phys. Rev. B **86**, 125441 (2012)
- [38] A. Luther and D.J. Scalapino, Phys. Rev. B **16**, 1153 (1977)
- [39] M. Levin and X.-G. Wen, Phys. Rev. Lett. **96**, 110405 (2006)
- [40] A. Kitaev and J. Preskill, Phys. Rev. Lett. **96**, 110404 (2006)
- [41] D.M. Basko, I.L. Aleiner, and B.L. Altshuler, Ann. Phys. (N.Y.) **321**, 1126 (2006)
- [42] B. Bauer and C. Nayak, Phys. Rev. X **4**, 041021 (2014)
- [43] J.H. Bardarson, F. Pollmann, and J.E. Moore, Phys. Rev. Lett. **109**, 1 (2012)

